Experimental characterization and modelization of ion exchange kinetics for a carboxylic resin in infinite solution volume conditions. Application to monovalent–trivalent cations exchange

Sébastien Picart, Isabelle Ramière, Hamid Mokhtari, Isabelle Jobelin

Experimental characterization and modelization of ion exchange kinetics for a carboxylic resin in infinite solution volume conditions. Application to monovalent-trivalent cations exchange.

Sébastien Picart,[*,†] Isabelle Ramière,[*,‡] Hamid Mokhtari,[†] and Isabelle Jobelin[†]

CEA, Nuclear Energy Division

RadioChemistry and Processes Department, Actinides Chemistry and Conversion Laboratory,

F-30207 Bagnols-sur-Cèze, France, and

Fuel Study Department, Fuel Simulation Laboratory, F-13108 Saint-Paul-lez-Durance, France

E-mail: sebastien.picart@cea.fr; isabelle.ramiere@cea.fr

[*]To whom correspondence should be addressed
[†]RadioChemistry and Processes Department
[‡]Fuel Study Department

Abstract

This study is devoted to the characterization of ion exchange inside a microsphere of carboxylic resin. It aims at describing the kinetics of this exchange reaction which is known to be controlled by interdiffusion in the particle. The fractional attainment of equilibrium function of time depends on the concentration of the cations in the resin which can be modelized by the Nersnt Planck equation. A powerful approach for the numerical resolution of this equation is introduced in this paper. This modelling is based on the work of Helfferich but involves an implicit numerical scheme which reduces the computational cost. Knowing the diffusion coefficients of the cations in the resin and the radius of the spherical exchanger, the kinetics can be hence completely determined. When those diffusion parameters are missing, they can be deduced by fitting experimental data of fractional attainment of equilibrium. An efficient optimization tool coupled with the implicit resolution has been developed for this purpose. A monovalent/trivalent cation exchange had been experimentally characterized for a carboxylic resin. Diffusion coefficients and concentration profiles in the resin were then deduced through this new model.

1 Introduction

The carboxylic resins find numerous applications in daily life for the softening and demineralization of water but also in industry for the purification of metallurgical[1] or biological products[2]. Their outstanding properties are a very high exchange capacity and a strong selectivity between divalent (or trivalent) and monovalent cations [3]. Recently, those ion exchangers have been studied for the removal of Fe(III) from an acid sulphate media representative of mining solutions and effluents[4] or for analytical purpose concerning the determination of U(VI) in environmental samples[5]. However, their applications to the field of materials have been investigated to a lesser extent. Yet, the loading of a spherical cation exchanger by a lanthanide or an actinide cation followed by its carbonisation can be an interesting way to obtain perfect microsphere of lanthanide or actinide oxide[6,7]. This process was successfully exploited to produce kernels of uranium oxide or carbide

for the nuclear fuel of high temperature gas reactor[8,9] and stands for an alternative route to sol-gel process[10] or infiltration method[11]. For this purpose, the saturation of the resin by a lanthanide cation is required and the kinetics of the loading operation has to be perfectly mastered. Few studies are devoted to this subject. We are then interested in a full comprehensive understanding of the exchange rate between the monovalent counter-ion of the resin and the lanthanide cation present in solution[12].

Only few studies are devoted to the in-depth modelling of the kinetics of the ion exchange. Most of the time, adsorption models with first-order kinetics are used[13]. In some particular situations, e.g. isotopic exchanges[14], an analytical solution describing the time evolution of the concentration in the resin can be obtained. Hence the kinetics of the exchange can be totally determined. Generally speaking, the full understanding of the exchange requires numerical resolutions. In the conditions of relatively high concentration in solution (0,1-0,5 mol/L), the limiting step of the reaction is the interdiffusion process in the microsphere (intraparticle diffusion) instead of the film diffusion phenomena. The interpretation of this particular diffusion of charged species in an ionic polymer is obtained from the numerical resolution of the Nernst-Planck equation. Those concepts and explicit calculations were first exposed by Helfferich and co-workers[15] who succeeded in describing the evolution of the fractional attainment of equilibrium with time for monovalent and divalent cations characterized by different diffusion coefficients. For practical purposes (mainly based on calculation times), we propose here to use an implicit resolution of the Nernst-Planck equation. This implicit resolution is based on a semi-implicit scheme that enables us to obtain a linear system that can be easily solved. Otherwise fully implicit schemes applied to the Nernst-Planck equation lead to a non-linear system to be solved, which implies an iterative resolution where a linear system is solved at each step, see for example the recent application for liquid junctions in[16].

The novelty of this article is then to determine self diffusion coefficients of both partners from experimental data through an optimization procedure based on the semi-implicit resolution Nernst-Planck equation. This optimization process is first validated by treating some data from the literature for monovalent/monovalent exchanges. The method was then applied to the proton/ammonium

and the ammonium/neodymium exchange. To the best of our knowledge, it is the first full modelling of a monovalent/trivalent exchange.

2 Experimental: Materials and procedure

2.1 Preparation of materials

2.1.1 Screening of the resin

The ion exchange material employed in this investigation was an acrylic resinous exchanger in its proton form, from Rohm & Haas Company (Chauny, France), called IMAC HP 333. Because the particle size is of importance for kinetics, a mechanical wet screening was performed on a Retsch apparatus (Retsch, AS200 Basic) through successively finer standard sieves (Prolabo, $400\mu m/600\mu m/800\mu m/1000\mu m$). A final manual screening was operated on each size range with the same sieves by means of a brush under a stream of deionized water. The fraction of $600-800\mu m$ size was selected for our experiments.

2.1.2 Washing of the resin

The resin was first washed by repeated column equilibration with a $1M$ aqueous ammonia solution, deionized water, $1M$ aqueous nitric acid solution and deionized water (3 cycles). The capacity of the resin was checked at the third cycle by measuring the quantity of ammonium and proton exchanged: the analytical weight capacity is equal to 11.6 meq/g of dry H^+ resin and the technical volume capacity is about 3.7 meq/mL of resin bed[17]. Eventually, it was removed from the column and was dried at $105°C$ and stored dry in its proton form.

2.2 Cations Exchanges

All experiments were performed at room temperature ($20\pm2°$C).

2.2.1 Proton-Ammonium ion exchange rate measurements

The day of the experiment, a weight portion of H^+ form resin (about 30 *mg*) was introduced in a small column (BioRad, 5 *cm* high, 0.5 *cm* of diameter) and hydrated for 2 hours by contact with deionized water. The cell was flushed initially with deionized water to remove air bubbles. After a few minutes, a $0.3M\ NH_4NO_3$ (pH $\simeq$ 5) solution was passed through the shallow bed of absorbent (flow rate = $100mL/min$, Ismatec Reglo volumetric pump) for a given time t and followed by a water wash ($200mL$). The quantity of proton released in the filtrate $Q_H(t)$ was estimated from the change of pH between the feeding solution and the percolate (Metrohm Combined glass electrode) and from speciation simulation on proton, ammonia and nitrate using Jchess Program[18]. The amount of ammonium fixed in the resin, $Q_{NH_4}(t)$, is equivalent to $Q_H(t)$.

At last, a batch experiment was also carried out by contacting for 2 days a mass of 51.3 *mg* of proton form resin with 1 L of a 0.3 $mol/L\ NH_4NO_3$ solution. This experiment is useful to characterize the equilibrium.

2.2.2 Ammonium-Neodymium ion exchange rate measurements

A weight portion of NH_4^+ form resin (about 20 *mg*) was rehydrated for 2 hours by contact with 10 *mL* of a 1 $mmol/L\ NH_4NO_3$ solution and was placed in the same column as described before. Then a 0.1 $mol/L\ Nd(NO_3)_3$ aqueous solution was forced through the shallow resin bed for a determined time t at a fixed flow rate of 100 mL/min. After contact, the resin was thoroughly washed with of 200*m*L of deionized water. The amount of neodymium contained in the resin was measured by dissolution when getting back the Nd^{3+} cation into solution with an acid treatment (HNO_3 1 mol/L, volume = 2 *mL*) and measuring the concentration of the lanthanide cation by a spectrophotometric analysis. This quantity, named $Q_{Nd}(t)$, was expressed in μeq by multiplying the number of $\mu moles$ by the charge of Nd^{3+}, that is 3.The resin left was collected and dried at $105°C$ for 4 hours and then weighed. By multiplying the weight capacity by this mass, the total exchange capacity of the resin, Q_{max}, initially present in its ammonium form, was estimated.

As previously, a batch experiment was performed by equilibrating for 3 days a mass of 52.7 *mg* of

ammonium form resin (corresponding to 36.7 mg of proton form resin) with 1 L of a 0.1 mol/L $Nd(NO_3)_3$ solution. The Nd content in the resin was analyzed at equilibrium by dissolution in 5 mL HNO_3 1 mol/L solution.

3 Results

The results of the proton/ammonium exchange can be found in Table 1. The initial mass of the proton resin are reported as well as the quantity of proton released in the percolate from the pH analysis, which corresponds to the quantity of ions exchanged for a given time. The ratio of the amount of ammonium in the resin over the full exchange capacity, $Q_{NH_4}(t)/Q_{max} = Q_H(t)/Q_{max}$, represents the degree of conversion of the resin. From the batch experiment, the equilibrium is then considered to be achieved when the conversion of the resin reaches 16.5 %. The conversion is not complete because the feeding solution is slightly acid and the separation factor between proton and ammonium may be high. The fractional attainment of equilibrium F is then calculated by using the following relation

$$F(t) = \frac{\frac{Q_H(t)}{Q_{max}}}{\frac{Q_H^\infty}{Q_{max}^\infty}} \tag{1}$$

Table 1: Observed degree of conversion and fractional attainment of equilibrium for a proton/ammonium exchange on a IMAC-HP333 carboxylic resin ($r_0 = 350\ \mu m$).

t	RH	$pH\ initial$	$pH\ final$	$Q_H(t)$	Q_{max}	$\frac{Q_H(t)}{Q_{max}}$	$F(t)$
s	mg			$\mu\ eq$	$\mu\ eq$	%	%
20	29.6	5.01	3.78	6.4	343.4	1.9	11.4
52	29.2	5.01	3.90	12.3	338.7	3.6	22.2
117	29.5	5.01	4.11	16.3	342.2	4.8	29.1
308	24.9	4.99	4.46	20.3	288.8	7.0	42.9
597	28.9	5.01	4.50	35.8	335.2	10.7	65.2
900	29.0	5.01	4.63	36.9	336.4	11.0	67.0
1800	26.1	4.99	4.75	45.6	302.8	15.1	91.9
3000	30.1	5.11	4.93	54.2	349.2	15.5	94.7
172800	51.3	5.02	4.13	97.5	595.1	16.4	~ 100

The experimental results of the ammonium/neodymium exchange are given in Table 2. The initial mass of the ammonium resin and its equivalent proton mass measured after dissolution experiments and drying are reported as well as the concentration of Nd in the dissolution solution and the quantity of Nd fixed in the resin in μeq. As regards the result of the batch experiment, the resin is fully converted at equilibrium which means $(Q_{Nd}/Q_{max})^{\infty} = 1$. Hence, the fractional attainment of equilibrium is directly given by the ratio of the amount of Nd in the resin over the exchange capacity, $Q_{Nd}(t)/Q_{max}$.

$$F(t) = \frac{Q_{Nd}(t)}{Q_{max}} \tag{2}$$

Table 2: Observed degree of conversion and fractional attainment of equilibrium for an ammonium/neodymium exchange on a IMAC-HP333 carboxylic resin ($r_0 = 350\ \mu m$).

t	RH	$[Nd]$	$Q_{Nd}(t)$	Q_{max}	$F(t)$
s	mg	$mmol/L$	$\mu\ eq$	$\mu\ eq$	%
60	15.7	3.6	21.5	181.7	11.8
120	16.0	6.2	37.4	185.5	20.2
300	16.3	9.8	58.7	189.0	31.1
600	14.9	11.6	69.8	172.6	40.4
1200	14.7	16.2	97.0	170.1	57.0
2400	9.5	13.8	82.8	110.2	75.1
3050	18.6	28.4	170.4	215.8	79.0
259200	36.7	27.8	417.0	425.7	~ 100

For the two systems, the relative uncertainty of measurement on F(t) stems essentially from the weighing operations of the resin and was estimated at 7%.

4 Modelling of the ion exchange

4.1 Formulation of the problem

We consider the ion exchange between spherical resin beads of uniform size in contact with a well-stirred solution. The exchange process is controlled by the interdiffusion of the species A and

B, either in the resin particle or in the diffusion layer adherent to the resin particle. In this paper, only the case of particle control is treated which corresponds to experimental conditions of efficient stirring, large diameter of the resin and relatively concentrated solution[19] ($> 100\ mmol/L$). An empirical criterion defined by Helfferich[20] allows to predict the nature of the rate-determining step for complete conversion, infinite solution volume and counter ions of equal mobility. However this calculation requires the value of the interdiffusion coefficient in the ion exchanger which is unknown for the type of carboxylic resin considered here. This study, as we will see in section Section 6.1, aims at determining the individual diffusion coefficients in the resin which will enable to calculate this criterion and verify *a posteriori* that the hypothesis of particle control diffusion was well-founded.

The gradient of the chemical potential of one specie is the driving force of its flux. This flux not only consists in the concentration gradient but it also consists in the gradient of the electrical potential which is a result of the diffusion process. Under some symplifying assumptions, Nernst-Planck equations[21,22] are well adapted to describe this ionic interdiffusion processes in the resin. These assumptions, usually encountered for the modelling of ion exchange kinetics[15,23], are listed below:

- The resin is considered as a homogeneous phase regardless its porous structure. It is spherical in shape so that we restrict to radial diffusion,
- The individual diffusion coefficients are constant for a given resin whatever is the resin's composition,
- The concentration of ionogenic groups (carboxylate function) troughout the resin is assumed to be constant. The changes in swelling are not being taken into account,
- The concentration and flux of co-ions (anions in our case) in the resin is neglected because the concentration of fixed ionic group in the resin is relatively high so that co-ions are excluded according to the Donnan effect.

Then, combining the Nernst-Planck equations describing the fluxes of two counter ion species A and B into the resin with the electroneutrality of the system and the no charge accumulation, we obtain the following flux

$$\Phi_A = -\left[\frac{D_A D_B\left(z_A^2 C_A + z_B^2 C_B\right)}{D_A z_A^2 C_A + D_B z_B^2 C_B}\right]\nabla C_A, \tag{3}$$

where the subscripts A and B refer to the counter ion species, D is the individual diffusion coefficient, C is the molar concentration and z is the electrochemical valence.

The quantity in brackets is designed as the "interdiffusion coefficient" in the literature (see e.g. Ref. 15) and is often denoted by D_{AB}.

Then for time-dependent processes, the Fick equation (or continuity equation) reads

$$\frac{\partial C_A}{\partial t} = -\nabla.\Phi_A$$

As we are interested by an interdiffusion process between a solution and a spherical resin, the previous equation is transposed in spherical coordinates. As the resin presents a radial symmetry (see above assumptions), we have

$$\frac{\partial C_A}{\partial t} = \frac{1}{r^2}\frac{\partial}{\partial r}\left(r^2\left[\frac{D_A D_B\left(z_A^2 C_A + z_B^2 C_B\right)}{D_A z_A^2 C_A + D_B z_B^2 C_B}\right]\frac{\partial C_A}{\partial r}\right).$$

where t is the time and r is the radial coordinate. This equation is defined at all point of the resin.

To finish, in a dimensionless and conservative form, the interdiffusion process is described by the following partial differential equation (PDE)

$$\frac{\partial \gamma_A}{\partial \tau} - \frac{1}{\rho^2}\frac{\partial}{\partial \rho}\left(\frac{1+b\gamma_A}{1+a\gamma_A}\rho^2\frac{\partial \gamma_A}{\partial \rho}\right) = 0, \qquad \forall \rho \in [0,1[,\ \tau \in \mathbb{R}^+ \tag{4}$$

with the dimensionless variables and parameters defined by

$$\gamma_A \equiv \frac{z_A C_A}{C_{max}},\ \tau \equiv D_A \frac{t}{r_0^2},\ \rho \equiv \frac{r}{r_0},\ a \equiv \frac{z_A D_A}{z_B D_B} - 1,\ b \equiv \frac{z_A}{z_B} - 1$$

where r_0 represents the microspherical resin radius and $C_{max} = z_A C_A + z_B C_B$ is the total equivalent concentration which is constant since there is no charge accumulation. Then $\gamma_A + \gamma_B = 1$ with $0 \leq \gamma_A, \gamma_B \leq 1$.

The previous PDE holds whatever the subscript A designs the ion adsorbed by the resin or the ion rejected in the solution. The choice of the counter ion A influences only the boundary and initial conditions of the problem to be solved.

The initial condition corresponds to the initial dimensionless concentration of the specie A in the resin. This initial concentration is supposed to be uniform is the resin:

$$\gamma_A(\rho, 0) = \gamma_A^0, \quad \forall \rho \in [0, 1[\tag{5}$$

The boundary conditions read

$$\frac{\partial \gamma_A}{\partial \rho}|_{\rho=0} = 0, \quad \text{(radial symmetry)} \tag{6a}$$

$$\forall \tau > 0 \qquad \text{(surface concentration)}: \begin{cases} \star \textit{if } A = \textit{ion rejected in solution:} \\ \gamma_A(1^-, \tau) = 1 - \lambda + \lambda \gamma_A(1^+, \tau) \\ \star \textit{if } A = \textit{ion adsorbed by the resin:} \\ \gamma_A(1^-, \tau) = \lambda \gamma_A(1^+, \tau) \end{cases} \tag{6b}$$

where $\gamma_A(1^-, \tau) = \lim_{\rho \to 1^-} \gamma_A(\rho, \tau)$, $\gamma_A(1^+, \tau) = \lim_{\rho \to 1^+} \gamma_A(\rho, \tau)$ and λ is the distribution ratio of the resin for the counter ion adsorbed. The first expression of the internal concentration $\gamma_A(1^-, \tau)$ at

the surface of the resin is obtained using $\gamma_A + \gamma_B = 1$ in the expression of λ recalled in Eq. (7)

$$\lambda = \frac{\gamma_{ad}(1^-, \tau)}{\gamma_{ad}(1^+, \tau)}, \qquad \forall \tau > 0 \tag{7}$$

where the subscript *ad* designs the ion adsorbed by the resin. This distribution ratio is constant in time.

As the concentrations in solution are considered to be homogeneous, we have $\gamma_A(1^+, \tau) = \gamma_A(\rho > 1, \tau)$. Moreover, in the infinite solution volume case, which is of interest here, the concentration in solution is also constant in time due to the continuous renewal of the solution

$$\gamma_A(\rho > 1, \tau) = \gamma_A^S, \quad \forall \tau \geq 0 \tag{8}$$

Then, boundary condition (6b) becomes

$$\gamma_A(1^-, \tau) = \gamma_A^\infty = \begin{cases} 1 - \lambda + \lambda \gamma_A^S & \text{if } B = ad \\ \lambda \gamma_A^S & \text{if } A = ad \end{cases} \qquad \forall \tau > 0 \tag{9}$$

Eq. (9) enables us to conclude that the concentrations of counters ions at the surface of the resin are constant in time for $\tau > 0$ in the infinite volume solution case.

Remark: *A distribution ratio of the resin equal to* 1 *leads to the continuity of the concentrations through the surface of the resin:* $\gamma_A(1^-, \tau) = \gamma_A(1^+, \tau), \forall \tau > 0$.

Example: *Assuming that initially the resin contains counter ions A only and the infinite volume solution contains counter ions B only, we have* $B = ad$ *and*

$$\gamma_A^0 = 1, \quad \gamma_A^S = 0 \quad \textit{and hence} \quad \gamma_A^\infty = 1 - \lambda$$

The solution $\gamma_A(\rho,\tau)$ of Eq. (4) enables us to calculate the fractional attainment of equilibrium f at each dimensionless time by:

$$f(\tau) = \frac{q_A^0 - q_A(\tau)}{q_A^0 - q_A^\infty} \tag{10}$$

where $q_A(\tau)$ represents the amount of the specie A still present in the unit sphere at the dimensionless time τ, $q_A^0 = q_A(\tau = 0)$ and $q_A^\infty = q_A(\tau = \infty)$ (where infinity means the equilibrium state).

$$q_A(\tau) = 4\pi \int_0^1 \gamma_A(\rho,\tau)\rho^2 \, \mathrm{d}\rho, \tag{11}$$

and then

$$f(\tau) = \frac{\gamma_A^0 - 3\int_0^1 \gamma_A(\rho,\tau)\rho^2 \, \mathrm{d}\rho}{\gamma_A^0 - \gamma_A^\infty} \tag{12}$$

With this definition, we have

$$F(t) = f(\tau = D_A \frac{t}{r_0^2}) \tag{13}$$

where $F(t)$ is the fractional attainment of equilibrium at the time t expressed with non-dimensionless variables.

Remark : *As* $\gamma_A + \gamma_B = 1$, *we have*

$$q_A(\tau) + q_B(\tau) = q_{max}$$

where $q_{max} = \dfrac{4\pi}{3}$ *is the volume of the unit sphere.*
Hence, another definition of the fractional attainment of equilibrium is

$$f(\tau) = \frac{q_B^0 - q_B(\tau)}{q_B^0 - q_B^\infty}$$

As usually $q_B^0 = 0$*, the expression of the fractional attainment of equilibrium becomes* $f(\tau) = \frac{q_B(\tau)}{q_B^\infty}$ *and then returns to Eqs.(1) and (2) with the temporal transformation* $\tau = D_A \frac{t}{r_0^2}$.

4.2 Implicit numerical resolution

4.2.1 Notations

In the sequel, the following notations are used for the discretization in space and time. The domain $[0,1] \times [0, \tau_{max}]$ is discretized with a constant space step $\Delta\rho$ and a constant time step $\Delta\tau$ defined by

$$\Delta\rho = \frac{1}{N_i + 1}, \qquad \Delta\tau = \frac{\tau_{max}}{N_n} \tag{14}$$

where τ_{max} is the dimensionless simulation time ($\tau_{max} = D_a \frac{t_{max}}{r_0^2}$, with t_{max} the desired simulation time (in s)).

Hence, $N_i + 2$ equidistant discretization points are used in space while $N_n + 1$ equidistant discretization points are used in time. The nodes of the regular mesh are designed by

$$(\rho_i, \tau_n) = (i\Delta\rho, n\Delta\tau) \quad \forall i \in \{0, .., N_i + 1\}, \forall n \in \{0, .., N_n\} \tag{15}$$

As the space discretization concerns the resin only, the discrete point $\rho_{N_i+1} = 1$ represents the interior surface point.

Then γ_i^n denotes the approximation of the exact solution γ_A at the node (ρ_i, τ_n) and γ^n the discrete solution vector at time τ_n: $\gamma^n = (\gamma_i^n)_{i \in \{0,..,N_i+1\}}$

4.2.2 A semi-implicit Euler finite difference scheme

In their publications, Hellferich *et al.*[15,23] use finite differences to numerically solve Eq. (4). An explicit Euler numerical scheme (also called forward Euler scheme) is performed in time. In explicit time-marching schemes, at each space node the discrete solution at the new time is directly obtained from the solution at previous times. For example, the explicit Euler scheme applied to the

PDE described in Eq. (4) reads for the time step $\Delta\tau = \tau_n - \tau_{n-1}$, $n > 0$

$$\frac{\gamma^n - \gamma^{n-1}}{\Delta\tau} - \frac{1}{\rho^2}\frac{\partial}{\partial\rho}\left(\frac{1+b\gamma^{n-1}}{1+a\gamma^{n-1}}\rho^2\frac{\partial\gamma^{n-1}}{\partial\rho}\right) = 0. \tag{16}$$

The numerical solution γ^n is easily obtained at each time step. However, the main drawback of this approach is that the time step is limiting by the space step through the so-called CFL condition[24] to have a stable numerical algorithm. The resulting calculation times may become very important. We decide to use an implicit Euler time scheme (also called backward Euler scheme), for which a system has to be solved to obtain the solution at a current time with respect to the solution at the previous time. For example, for the PDE (4) the implicit Euler scheme reads for $n > 0$

$$\frac{\gamma^n - \gamma^{n-1}}{\Delta\tau} - \frac{1}{\rho^2}\frac{\partial}{\partial\rho}\left(\frac{1+b\gamma^{n}}{1+a\gamma^{n}}\rho^2\frac{\partial\gamma^{n}}{\partial\rho}\right) = 0. \tag{17}$$

In Eq. (17), the discretization of the space operators will lead to solve a system in order to obtain γ^n. In implicit time-marching schemes, the stability condition is less restraining than for explicit schemes. Larger time steps can thus be used. For some kind of PDE (linear for example) and space discretization (centered finite difference for example), the Euler implicit scheme is unconditionally stable: the time step and the space step are independent. Therefore, even if this approach requires an extra computation (resolution of a system at each time step), accurate solutions are obtained in much less computational time than for an explicit method. Both Euler time-marching schemes are of first-order in time.

As the PDE under study (see Eq. (4)) is non-linear, the fully implicit scheme leads to a non-linear system to be solved (cf. Eq. (17)). At each time step, an iterative procedure has then to be performed to obtain the solution. This non-linear resolution can become really costly. In order to solve a linear system at each time step, for which efficient and fast numerical methods can be applied, we decide to use a semi-implicit scheme. This semi-implicit scheme consists in applying the Euler implicit scheme on the PDE (4) with an explicit discrete diffusion coefficient. This explicit discrete coefficient is obtained evaluating the diffusion coefficient with the solution at the

previous time. The semi-implicit time scheme writes

$$\frac{\gamma^n-\gamma^{n-1}}{\Delta\tau}-\frac{1}{\rho^2}\frac{\partial}{\partial\rho}\left(\frac{1+b\gamma^{n-1}}{1+a\gamma^{n-1}}\rho^2\frac{\partial\gamma^n}{\partial\rho}\right)=0. \tag{18}$$

This scheme is still first-order accurate in time.

The initial approximation $\gamma^0=(\gamma_i^0)_{i\in\{0,..,N_i+1\}}$ is deduced from the initial condition (5). As the characteristic time required to reach the distribution ratio of the resin is negligible compared to the discretization time, we consider that the initial solution respects the boundary condition (6b). Thus, we set

$$\gamma_i^0=\gamma_A^0, \qquad \forall i\in\{0,..,N_i\}, \tag{19}$$

$$\gamma_{N_i+1}^0=\gamma_A^\infty. \tag{20}$$

Therefore, only N_n vectors γ^n ($n\in\{1,..,N_n\}$) have to be determined.

4.2.3 A centered space finite difference scheme

In space, we use the same second-order centered finite difference for the gradient than Helfferich

$$\left.\frac{\partial J^n}{\partial\rho}\right|_{\rho_i}\approx\frac{J^n_{i+\frac{1}{2}}-J^n_{i-\frac{1}{2}}}{\Delta\rho}, \quad \forall i\in\{1,..,N_i\},\forall n\in\{0,..,N_n\}. \tag{21}$$

where J denotes here either $\frac{1+b\gamma^{n-1}}{1+a\gamma^{n-1}}\rho^2\frac{\partial\gamma^n}{\partial\rho}$ or γ^n. At each time step $\Delta\tau=\tau_n-\tau_{n-1}$, the diffusion term $-\frac{1}{\rho^2}\frac{\partial}{\partial\rho}\left(\frac{1+b\gamma^{n-1}}{1+a\gamma^{n-1}}\rho^2\frac{\partial\gamma^n}{\partial\rho}\right)$ is then discretized by

$$-\frac{1}{\Delta\rho}\left(\frac{1+b\gamma^{n-1}_{i+\frac{1}{2}}}{1+a\gamma^{n-1}_{i+\frac{1}{2}}}\left(\frac{\rho_i+\frac{1}{2}\Delta\rho}{\rho_i}\right)^2\frac{\gamma^n_{i+1}-\gamma^n_i}{\Delta\rho}\right.$$
$$\left.-\frac{1+b\gamma^{n-1}_{i-\frac{1}{2}}}{1+a\gamma^{n-1}_{i-\frac{1}{2}}}\left(\frac{\rho_i-\frac{1}{2}\Delta\rho}{\rho_i}\right)^2\frac{\gamma^n_i-\gamma^n_{i-1}}{\Delta\rho}\right), \quad \forall i\in\{1,..,N_i\} \tag{22}$$

The estimation of $\gamma_{i+\frac{1}{2}}^{n-1}$ (resp. $\gamma_{i-\frac{1}{2}}^{n-1}$) is obtained by linear interpolation between γ_i^{n-1} and γ_{i+1}^{n-1} (resp. γ_i^{n-1} and γ_{i-1}^{n-1}) which is consistant with the second-order space discretization scheme.

The boundary conditions (6) are used to obtain the discretization scheme at the nodes ρ_0 and ρ_{N_i+1}. At $\rho_0(=0)$, we use a first-order discretization of the homogeneous Neumann condition

$$\frac{\gamma_1^n - \gamma_0^n}{\Delta\rho} = 0, \qquad \forall n \in 0,..,N_n \tag{23}$$

As the space finite difference scheme is second-order accurate, this first-order discretization causes a little lost of precision near the boundary. However the L^2 error-norm on the solution will remain of second-order in space. Eq. (23) leads to $\gamma_0^n = \gamma_1^n$, which enables us to eliminate γ_0^n of the unknowns vector.

The Dirichlet boundary condition (6b) applied at ρ_{N_i+1} (=1) gives directly the discrete solution at this node

$$\gamma_{N_i+1}^n = \gamma_A^\infty, \qquad \forall n \in 0,..,N_n \tag{24}$$

Hence, at each time step only N_i space unknowns ($i \in \{1,..,N_i\}$) have to be determined.

4.2.4 Linear evolution system

The linear system of dimension $N_i \times N_i$ to be solved at each time step $\Delta\tau = \tau_n - \tau_{n-1}$ writes

$$M\ G = F \tag{25}$$

where the matrix M of the system is tridiagonal. In the sequel, $D_M(i)$ will denote the diagonal term of M at row i, $U_M(i)$ the upper-diagonal term and $L_M(i)$ the lower-diagonal term. The unknown vector G corresponds to the solution γ^n for nodes $i \in \{1,..,N_i\}$. The right hand side F results from the time discretization and the boundary conditions, as detailed below.

For $1 < i < N_i$, the coefficients of the linear system (25) can be expressed by

$$D_M(i) = 1 + \frac{\Delta\tau}{(\Delta\rho)^2} \times (R_+(i)D_+(i,n) + R_-(i)D_-(i,n)) \quad (26)$$

$$U_M(i) = -\frac{\Delta\tau}{(\Delta\rho)^2} \times (R_+(i)D_+(i,n)) \quad (27)$$

$$L_M(i) = -\frac{\Delta\tau}{(\Delta\rho)^2} \times (R_-(i)D_-(i,n)) \quad (28)$$

$$F(i) = \gamma_i^{n-1} \quad (29)$$

where the notations R_+, R_-, D_+ and D_- are those of Hellferich *et al.*[15,23] defined $\forall i \in \{1,..,N_i\}$

$$R_+(i) = \left(\frac{\rho_i + \frac{1}{2}\Delta\rho}{\rho_i}\right)^2, \qquad R_-(i) = \left(\frac{\rho_i - \frac{1}{2}\Delta\rho}{\rho_i}\right)^2 \quad (30)$$

$$D_+(i,n) = \frac{2 + b(\gamma_{i+1}^{n-1} + \gamma_i^{n-1})}{2 + a(\gamma_{i+1}^{n-1} + \gamma_i^{n-1})}, \qquad D_-(i,n) = \frac{2 + b(\gamma_i^{n-1} + \gamma_{i-1}^{n-1})}{2 + a(\gamma_i^{n-1} + \gamma_{i-1}^{n-1})} \quad (31)$$

As $R_+(i) \neq R_-(i+1)$, the matrix M is non-symmetric.

For the indexes $i = 1$ and $i = N_i$, there are special terms coming from the discretization of the boundary conditions. At $i = 1$, the discretization of the Neumann boundary condition (23) enables us to determine the terms of the matrix and the right hand side

$$D_M(1) = 1 + \frac{\Delta\tau}{(\Delta\rho)^2} \times (R_+(1)D_+(1,n)), \quad (32)$$

$$U_M(1) = -\frac{\Delta\tau}{(\Delta\rho)^2} \times (R_+(1)D_+(1,n)), \quad (33)$$

$$F(1) = \gamma_1^{n-1} \quad (34)$$

As $i = 1$ is the first index of the unknown vector G, the matrix M does not contain any lower-diagonal term.

For $i = N_i$ there is no upper-diagonal term. The contribution of the Dirichlet condition at the last

space indexed by $i = N_i + 1$ (cf. Eq. (24)) is taken into account thanks to the right hand term $F(N_i)$.

$$F(N_i) \quad = \quad \gamma_{N_i}^{n-1} + \frac{\Delta\tau}{(\Delta\rho)^2} \times (R_+(N_i) D_+(N_i, n)) \times \gamma_A^\infty \tag{35}$$

The diagonal term $D_M(N_i)$ and the lower-diagonal term $L_M(N_i)$ are simply obtained using Eqs.(26) and (28) with $i = N_i$.

Usual techniques (e.g. Ref. 25) enables us to conclude that this semi-implicit scheme converges to the solution of the continuous problem (4). We get a first-order accuracy in time and second-order accuracy in space. Moreover this scheme is unconditionally stable. The choice of the time and space steps will thus only depend on the desired precision, see Section 5.2. As this scheme verifies the maximum principle, we have $\forall n \geq 0$ and $\forall i \in \{0, .., N_i + 1\}$

$$\min(\gamma_A^\infty, \gamma_A^0) \leq \gamma_i^n \leq \max(\gamma_A^\infty, \gamma_A^0) \tag{36}$$

4.3 Determination of optimal individual diffusion coefficients by a refinement procedure

In practical case, one has to determine the diffusion coefficients of the counter species A et B from data of fractional attainment of equilibrium, cf. Section 3. The optimal diffusion coefficients are those that minimize the distance between the experimental data and the numerical fractional attainment of equilibrium obtained with these coefficients.

Classical optimization algorithms (gradient, Levenberg-Marquardt, ...) strongly depends on the starting values and requires many data to give a reliable estimation of the parameters. Unfortunately, we only have an idea of the order of magnitude of the diffusion coefficient which may not be enough to have a good starting point. Moreover, we have too few experimental data at our disposal (around 6 points to determine 2 diffusion coefficients) to use classical optimization methods. We decide to use a refinement procedure to find the optimal diffusion coefficients. The ground principle of this optimization process comes from multigrid methods[26]. It consists in a “in-depth”

research instead of a research of descent directions. When the problem under study leads to a sufficiently smooth behavior of the error with respect to the parameters to optimize (which is the case here), the algorithm by refinement has the main advantage to yield physical optimal parameters even if few data are given.

The optimization procedure by recursive refinements can be described by the following steps :

i) set initial variation intervals VI_A and VI_B for D_A and D_B,

ii) set a number of discretization points for each interval VI_A and VI_B. In each variation interval, the points are chosen to be equidistantly distributed. If a variation interval covers more than one power of 10, the equidistant distribution is made in the logarithm scale. This enables us to chose variation intervals covering several power of 10.

iii) for each node of the mesh of the domain $\mathrm{VI}_A \times \mathrm{VI}_B$:

   a- solve the PDE (4) with the semi-implicit numerical method described above. The diffusion coefficients D_A and D_B used for this resolution are the discrete values associated to the node under study,

   b- for each discrete time τ_n, $n \in \{0,..,N_n\}$, calculate the approximate fractional attainment of equilibrium thanks to Eq. (12). A quadrature formula is used to evaluate an approximation of the integral of γ_A from the discrete numerical solution $(\gamma_i^n)_{i\in\{1,..,N_i+1\}}$ obtained at step iiia,

   c- estimate the error on the fractional attainment from the experimental data. The time coordinate transformation has to be taken into account (see Eq. (13)). Interpolation techniques have often to be used in order to evaluate the discrete fractional attainment of equilibrium at each experimental time.

iv) determine the node of the mesh that yields to the minimal fractional attainment error.

v) test the stop criteria, which is typically based on the relative difference between two successive values of the error on the fractional attainment of equilibrium or on a maximal number of

iterations of the process.

a- if the stop criteria is verified, the 'minimization' node gives the optimal values of D_A and D_B,

b- else, determine new variation intervals VI_A and VI_B centered on the estimations of D_A and D_B associated to the minimization node. The bounds of the new intervals are chosen to be discrete values of the diffusion coefficients associated to the neighbor nodes of the minimization node. A special treatment is made when the minimization node is on the boundary of a variation interval. Then, this variation interval is enlarged in the concerned direction while the other variation interval is kept unchanged. Then, go back in iii.

A graphical representation of this procedure is given in Figure 1.

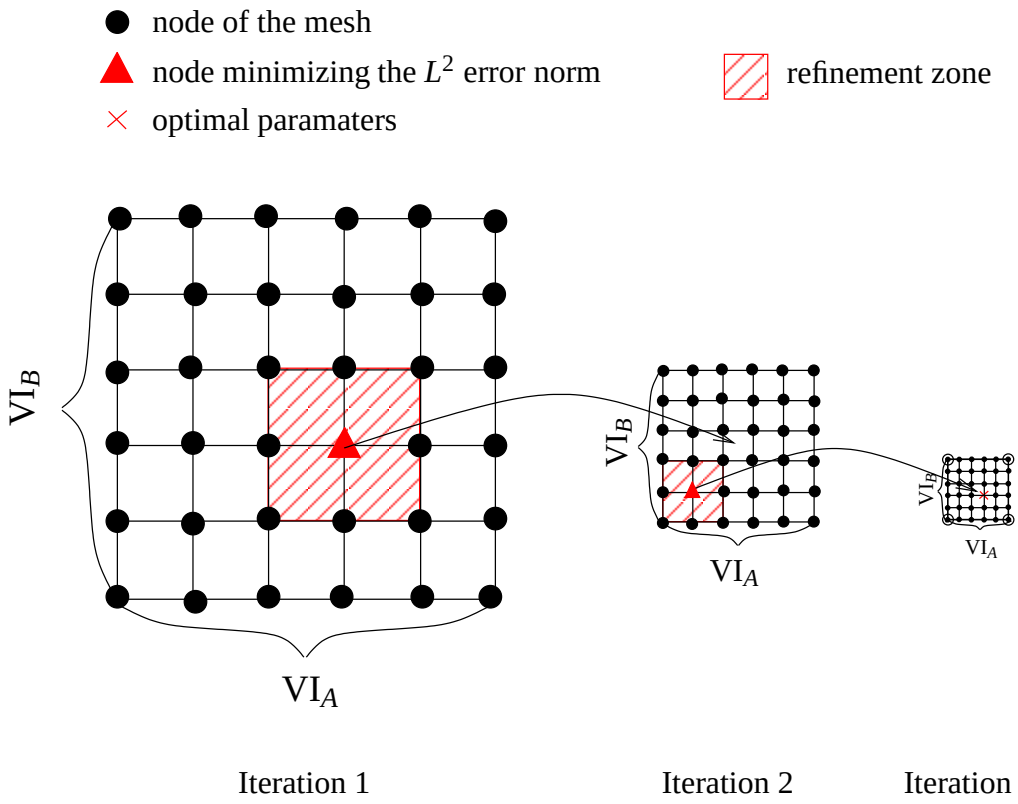

Figure 1: Refinement procedure to determinate optimal individual diffusion coefficients (obtained here within 3 iterations).

Thus, this algorithm consists in determining finer and finer variation intervals for D_A and D_B while

kipping the same number of discretization nodes for each interval: we are well in a recursive refinement procedure.

For this kind of optimization procedure consisting in performing many times the numerical scheme used to discretize the time- and space-dependent PDE, an implicit time-marching scheme is necessary to reach the optimal parameters within acceptable calculation times.

5 Numerical validation

5.1 Solver, norm and quadrature

The non-symmetric linear system (25) is solved using the Bi-CGSTAB algorithm[27]. This iterative solver has been optimized here for tridiagonal matrices.

At each time, the fractional attainment of equilibrium is computed as post-processing. To do this, the integral of the solution taking place in the expression of the fractional attainment of equilibrium (see Eq. (12)) is performed using a Simpson quadrature rule which is exact for polynomials of third order or less. An even number of constant subintervals is required to apply this formula.

The root mean square error (or deviation) on the fractional attainment of equilibrium is performed through the following expression:

$$e_F = \left(\frac{\sum_{d=1}^{nbpts} \left(F(t_d) - F_d\right)^2}{nbpts} \right)^{1/2} \tag{37}$$

where e_F denotes root mean square error on the fractional attainment of equilibrium F calculated from $nbpts$ experimental data. The index d refers to the data. Then $F(t_d)$ is the discrete fractional attainment of equilibrium evaluated at the experimental time t_d while F_d is the experimental fractional attainment of equilibrium at the same time. The error given by Eq. (37) is a good measure of the fitting precision.

The stop criterion of the optimization procedure is reached when the relative difference on the fractional attainment error is less than 1% between two iterations of refinement. This optimization process typically converges within 3 or 4 iterations. The maximal number of iterations is set to 20.

5.2 Validation of the semi-implicit approach

5.2.1 Precision and calculation times

First, the semi-implicit approach has been validated with respect to the results obtained with the explicit time discretization of Helfferich[15,23]. We consider a monovalent/monovalent ion exchange with individual diffusion coefficients in a ratio of $1/10$. The initial condition is $\gamma_A^0 = 1$ while the boundary condition at the surface of the resin is set at $\gamma_A^\infty = 0$. In this case, A designs the only ion initially present in the resin and that is rejected in the solution. On Figure 2, we compare the fractional attainment of equilibrium (cf. Eq. (12)) calculated from the solution obtained using the explicit scheme (we return to the results presented in Ref. 15) to the one obtained from the solution of the semi-implicit scheme described in (18).

For a fixed space step $\Delta\rho = 1/20$, the stability condition used for the explicit scheme leads to a time step $\Delta\tau = 1/10000$. As the semi-implicit scheme is unconditionally stable (see Section 4.2.4), the time step can be chosen arbitrarily. In this example we performed the semi-implicit scheme with $\Delta\tau = 1/200$ and $\Delta\tau = 1/500$. Consequently the resulting calculation times are reduced with the semi-implicit scheme. The main conclusions drawn from Figure 2 are the classical ones:

- the semi-implicit solution converges when the time step decreases,
- the main difference between the solutions obtained with the explicit or the implicit scheme are located at the beginning of the unsteady state (beginning of the ion exchange),
- the permanent solution ($\tau = \tau_{max}$) is the same whatever the time-marching scheme and the time step (it depends on the space step only).

In the sequel, the semi-implicit scheme will be performed in order to fit experimental data which are given within a relative precision about 7% and at experimental times leading to $\tau > 10^{-2}$. The

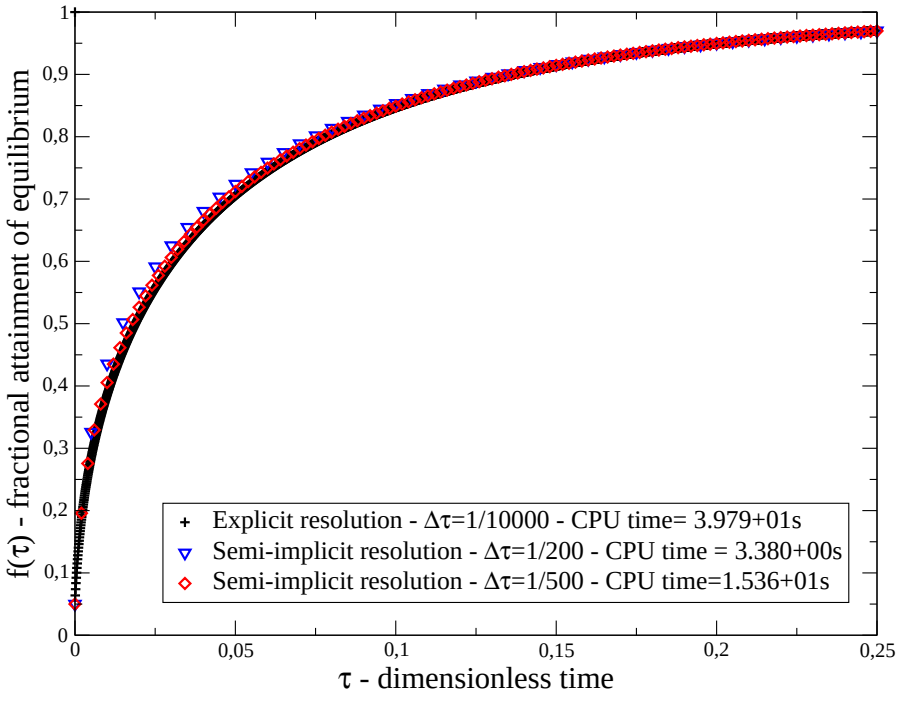

(a) Linear scale

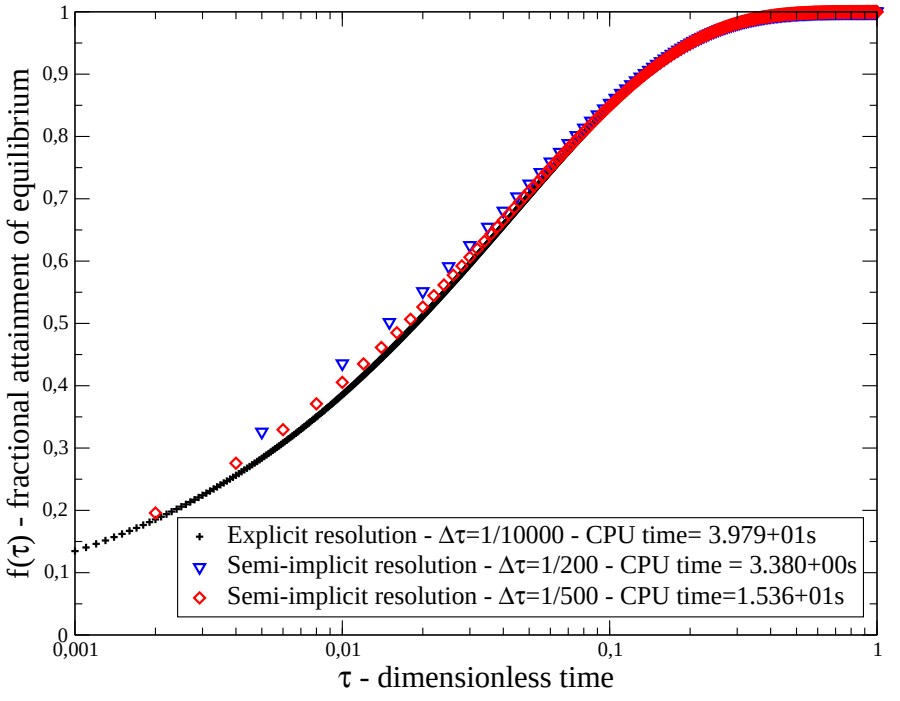

(b) Logarithm scale

Figure 2: Comparison of the semi-implicit and the explicit approaches for a monovalent/monovalent ion exchange.

comparison presented on Figure 2 enables us to conclude that the semi-implicit solution obtained with $N_n = 500$ is precise enough. In this case, the CPU time is improved by more than 60% with a semi-implicit approach instead of an explicit approach.

This confirms that for an optimization procedure, for which many resolutions are performed, the semi-implicit approach will reach the optimal solution within less computational time than the explicit approach.

5.2.2 Optimization procedure

The optimization method based on a refinement procedure was tested on experimental results from literature. The data was taken from Boyd and co-workers studies[14] on the kinetics of alcali metal cations exchange between chloride solutions and the ionic exchanger Amberlite IR-1 bearing methylene sulfonic acid groups[20]: it concerned the experiment R-3 describing the ion uptake of sodium used as a radioactive tracer ($8\ 10^{-5}$ M) from 0.111 M potassium chloride solutions at room temperature (30 °C). The resin, initially in its potassium form, exchanges its counter ions for sodium. If R denotes the resin, the reaction writes $RK + Na^+ \rightleftharpoons RNa + K^+$. The evolution of the fractional attainment of equilibrium with time is given in Table 3.

Table 3: Exchange of sodium ion from 0.1 M chloride solutions; Amberlite IR1 phenol-formaldehyde ionic exchanger; $r_0 = 0.0177\ cm$**;** $T = 30°\mathrm{C}$ **; composition of solution** $8\ 10^{-5}\ mol/L$ **NaCl,** $0.111\ mol/L$ **KCl; experiment R-3 from Ref. 14**

t (in s)	$F(t)$ (in %)
1.3	37.2
2.5	46.2
5.0	60.4
7.5	69.7
10.0	76.4
15	92.6
30	98.3
60	100

As the concentration in Na^+ is much smaller than the concentration in K^+, the interdiffusion coefficient assumes the individual diffusion coefficient of Na^+, cf. Eq. (3) and Ref. 20. The

optimization process will then yield to the optimal individual diffusion coefficient of Na^+ only. The analytical expression of the fractional attainment of equilibrium proposed by Boyd in[14] for an isotopic exchange can be used in this particular case since the interdiffusion coefficient returns to the diffusion coefficient of one counter ion only. Then, we have

$$F(t) = 1 - \frac{6}{\pi} \sum_{n=1}^{\infty} \frac{1}{n^2} \exp\left(- \frac{D_{Na^+} \pi^2 n^2 t}{r_0^2} \right) \tag{38}$$

As the counter ion of interest Na^+ is adsorbed by the resin, the interdiffusion equation (4) is solved with $A = ad$. Then, $\gamma_A^0 = 0$ and $\gamma_A^\infty = \lambda \gamma_A^S$. The dimensionless concentration of Na^+ in solution is obtained by $\gamma_A^S = \dfrac{8\ 10^{-5}}{0.111 + 8\ 10^{-5}} \simeq 7.2\ 10^{-4}$. The distribution ratio of the resin is considered to be equal to 1 since no selectivity of the resin is supposed between Na^+ and K^+ . Then $\gamma_A^\infty = 7.2\ 10^{-4}$. With an initial variation interval $[10^{-6}, 10^{-5}]$ divided into 10 subintervals for D_A, the optimization procedure converges within 3 iterations. The optimal diffusion coefficient of the sodium in the resin then obtained is $D_{Na^+} = 3.31\ 10^{-6}\ cm^2/s$ which is in good agreement with Boyd's value of $3.5\ 10^{-6}\ cm^2/s$. The root mean square error on the fractional attainment of equilibrium is then 0.0234. The analytical fractional attainment of equilibrium given in Eq. (38) applied to the diffusion coefficient obtained by Boyd ($D_{Na^+} = 3.5\ 10^{-6}\ cm^2/s$) yields for the same experimental data to an error of 0.0253 which is superior to the error obtained with the optimization process. Figure 3 enables us to appreciate the accuracy of the solution obtained with the optimization procedure. Furthermore, as in this case only one parameter has to be determined from 8 experimental data, a classical optimization procedure can be applied. The Levenberg-Marquardt algorithm leads to $D_{Na^+} = 3.34\ 10^{-6}\ cm^2/s$ which confirms the result obtained by our approach with recursive refinements.

This example confirms the validity and the accuracy of the optimization procedure by refinement introduced in this article.

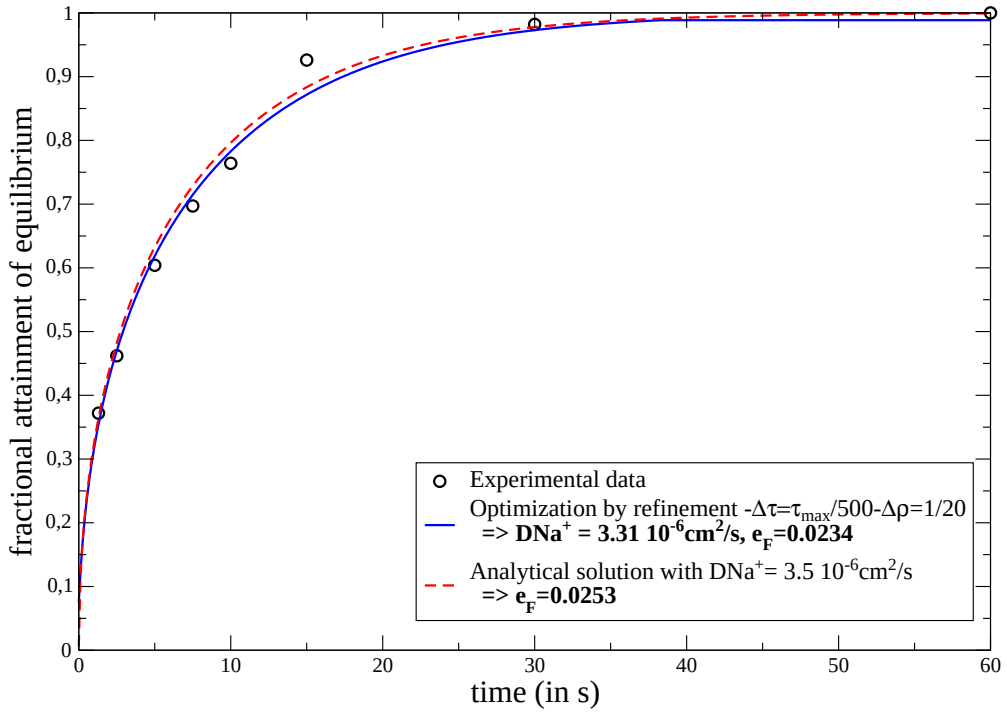

(a) Linear scale

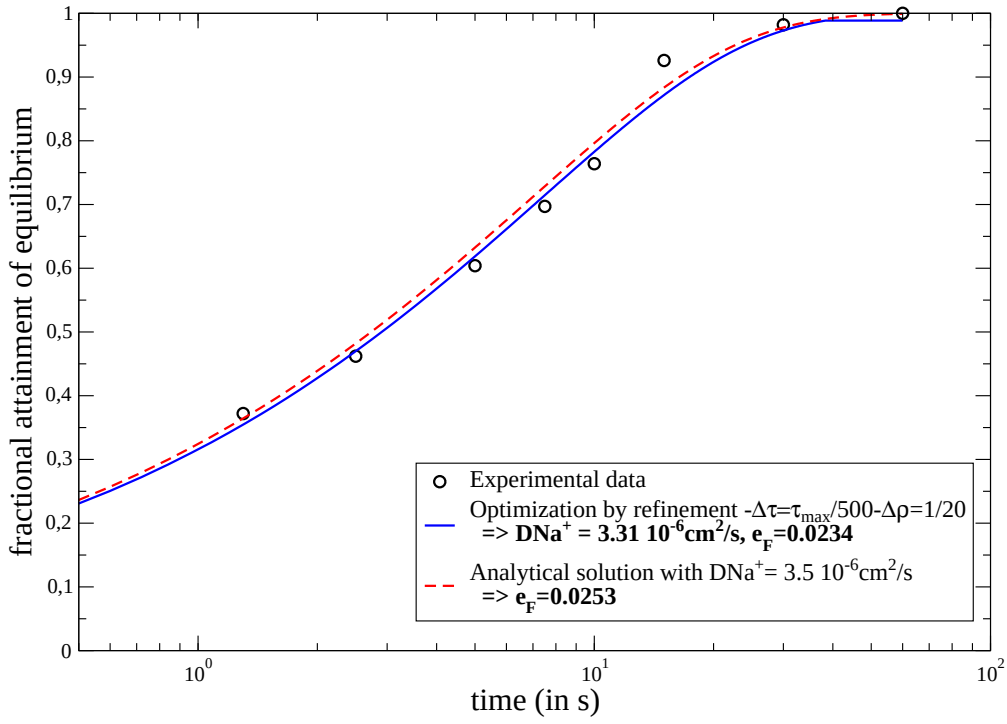

(b) Logarithm scale

Figure 3: Optimization procedure and analytical solution for the R-3 Boyd[14] experiment

6 Characterization of cation exchange in a carboxylic resin

6.1 Determination of individual diffusion coefficients

Using the experimental data given in section Section 3 of this article, the self diffusion coefficients of H^+, NH_4^+ and Nd^{3+} in the IMAC HP333 carboxylic resin were determined thanks to the optimization procedure. Knowing the diffusion rate of each cation, it was then possible to plot the radial concentration profile in the resin during the exchange for both examples.

In all the following optimizations, $N_i+2=21$ discretization points are used in space while $N_n+1=501$ discretization points are used in time. The variation intervals will consist of 11 discretization points (10 subintervals).

6.1.1 Proton/Ammonium exchange

For this first exchange, as the concentration of the rejected ion H^+ is measured, the optimization process is performed with $B=ad$. We have $\gamma_A^0=1$, $\gamma_A^S\simeq 0$ (negligible presence of proton in solution) and hence $\gamma_A^\infty=1-\lambda$. The distribution ratio of the resin is determined thanks to the data at equilibrium: $\lambda=0.164$. With initial variation intervals of $[10^{-8},10^{-6}]$ for D_{H^+} and $D_{NH_4^+}$, the optimal values of $D_{H^+}=1.58\ 10^{-7}\ cm^2s^{-1}$ and $D_{NH_4^+}=1.01\ 10^{-7}\ cm^2s^{-1}$ were obtained. They are typical values for monovalent cation diffusion encountered for example in cross-linked strong-acid cation exchanger[28]. Figure 4 shows the good agreement between the fractional attainment of equilibrium obtained with this coefficient and the experimental data from Table 1. The root mean square error is around $3\ 10^{-2}$.

The optimization process performed with $A=ad$ and hence $\gamma_A^0=0$, $\gamma_A^S=1$ and $\gamma_A^\infty=\lambda$ yields exactly the same optimal coefficients. It confirms that the optimization process is independent to the choice of the counter ion used for the dimensionless formulation (see Section 4.1).

If we consider the diffusion coefficients at infinite dilution of the ammonium and the proton in aqueous solution, $1.96\ 10^{-5}\ cm^2s^{-1}$ and $9.31\ 10^{-5}\ cm^2s^{-1}$ respectively[29], the diffusion rate of the proton was expected to be five times greater than the diffusion rate of the ammonium in the resin.

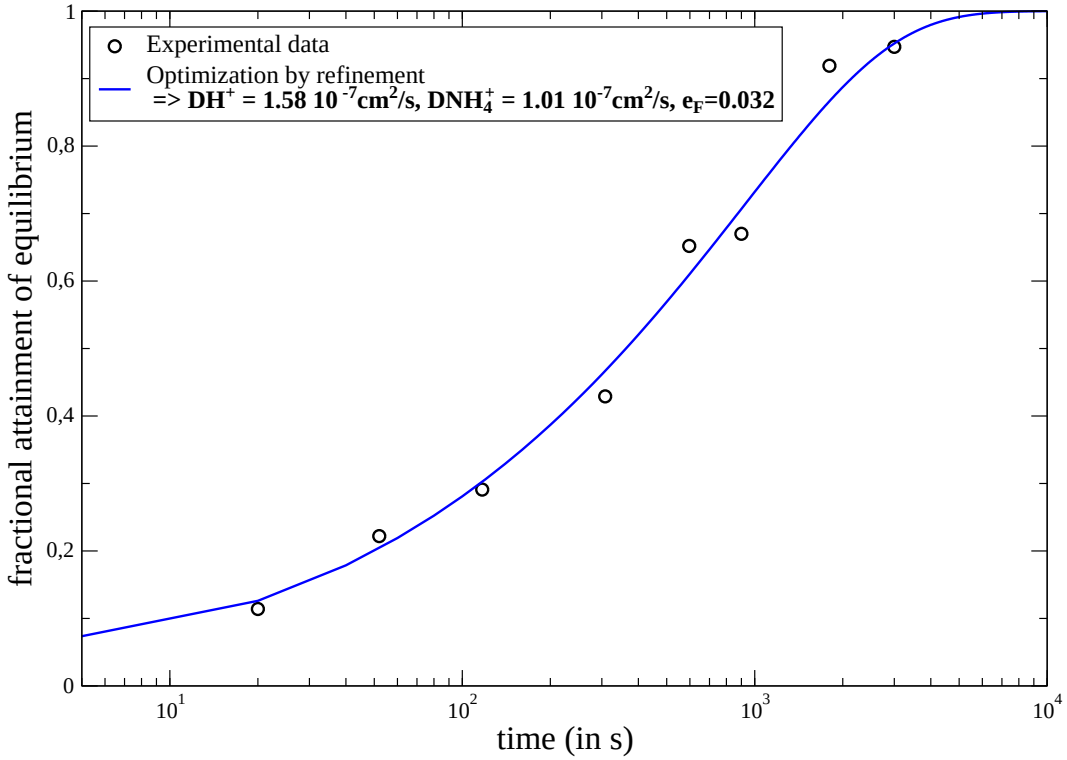

Figure 4: Fit of the fractional attainment of equilibrium for the proton/ammonium exchange. Experimental data given in Table 1.

It is in fact only almost two times bigger because of the large affinity that the proton possesses for the carboxylate group. Its specific chemical interaction surely diminishes its diffusivity in the resin in spite of its small size compared to ammonium. The interaction between ammonium and carboxylate groups is indeed essentially of an electrostatic nature which is less energetic.

6.1.2 Ammonium/Neodymium exchange

For this second case, the optimization scheme is performed as previously with a distribution ratio $\lambda = 1$ and initial variation intervals of $[10^{-8}, 10^{-6}]$ for $D_{NH_4^+}$ and $[10^{-9}, 10^{-7}]$ for $D_{Nd^{3+}}$. The diffusion coefficients of NH_4^+ and Nd^{3+} were estimated at 9.86 10^{-8} cm^2s^{-1} and 7.82 10^{-9} cm^2s^{-1} respectively. A graphical representation of the data fitting for the fractional attainment of equilibrium is given in Figure 5. The fitting error is better than for the proton/ammonium exchange (around 10^{-2}). The mobility of neodymium is less important than in solution where the diffusion

coefficient is equal to 6.16 $10^{-6} cm^2 s^{-1}$ (Ref. 29).

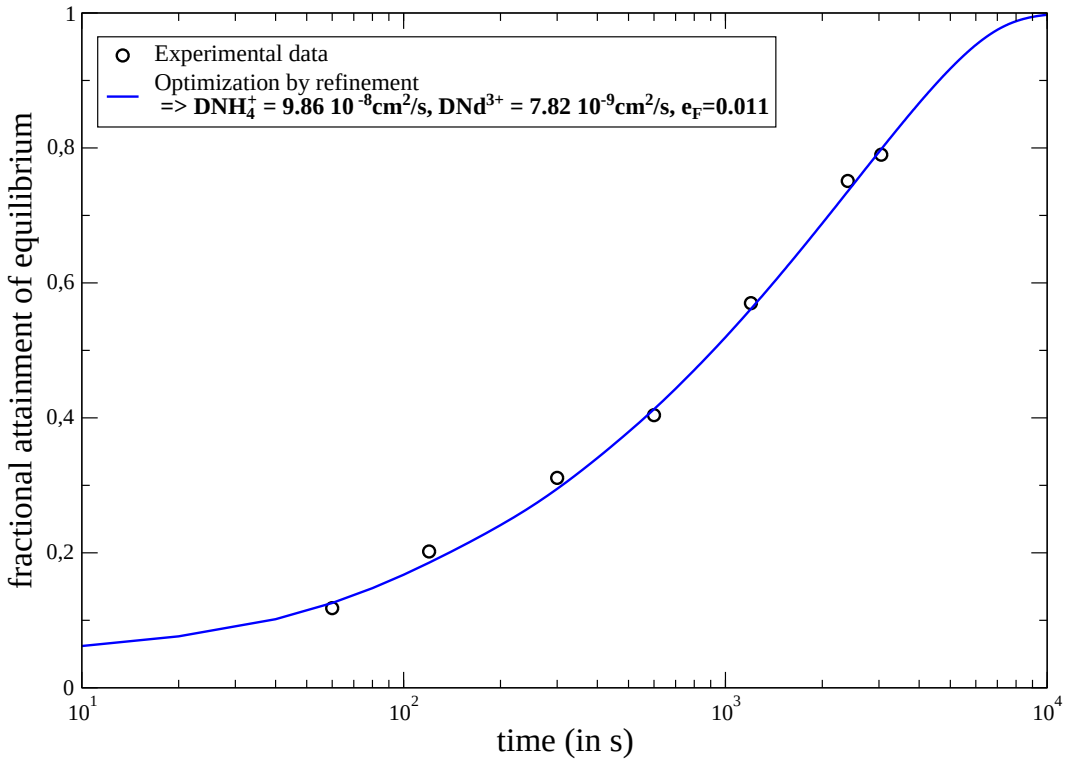

Figure 5: Fit of the fractional attainment of equilibrium for the ammonium/neodymium exchange. Experimental data given in Table 2.

The value of $D_{NH_4^+}$ found here coincides with the one determined for the proton/ammonium exchange: the average of the two values, ie 1 10^{-7} $cm^2 s^{-1}$, is then taken as the optimal value for the individual diffusion coefficient of the ammonium. Moreover, the diffusion rate for Nd^{3+} is less than for NH_4^+ and is comparable to values obtained by Soldano[30] for Y^{3+} in a 5 % cross-linked sulfonated polystyrene exchanger. The effect of charge upon diffusion rate is naturally strong because the electrostatic force fields exert a great influence on the movement of cations in the resin. In Table 4 are shown the values of self diffusion coefficient of the three different cations studied in the carboxylic resin. These results confirm that the full conversion time deeply depends on the orders of magnitude of both diffusion coefficients. The notion of interdiffusion coefficients is then of primary importance and rules the kinetic of the exchange. In our examples, a full attainment of equilibrium will take 7500 s for the H^+/NH_4^+ conversion ($D \sim 10^{-7}$ $cm^2 s^{-1}$) and 10000 s for the

Table 4: Self diffusion coefficients of cations in the IMAC-HP333 carboxylic resin; $T = 20°\mathrm{C}$

ion	D $(10^{-7}\ cm^2 s^{-1})$
H^+	1.6
NH_4^+	1.0
Nd^{3+}	0.08

NH_4^+/Nd^{3+} conversion ($D \sim 10^{-8} - 10^{-7}\ cm^2 s^{-1}$) for beads of radius of 350 μm at 20°C.

Remark The criterion for the rate-determining step mentioned in Section 4.1 and proposed by Helfferich[20] for complete conversion experiments is based on the ratio

$$\frac{C_{res} D_{res} \delta}{C_{sol} D_{sol} r_0}(5 + 2\alpha_B^A) \tag{39}$$

where C_{res} is the concentration of fixed ionic groups in the resin, D_{res} is the interdiffusion coefficient in the ion exchanger, δ is the film thickness, C_{sol} is the concentration in solution in equivalents, D_{sol} is the interdiffusion coefficient in the film, r_0 is the bead radius and α_B^A is the separation factor (A represents here the rejected ion). If this ratio is lower than 1, the exchange is controlled by particle diffusion. Otherwise, we have a film diffusion control.

This ratio can only be estimated in the case of the ammonium-neodymium exchange because only this exchange is complete. In details, a batch experiment was preliminary performed to estimate the separation factor α_B^A which consisted in contacting a 0.257 mol/L $Nd(NO_3)_3$ solution with 1.16 g of ammonium form resin and measuring the concentrations of both cations in solution and in the resin at equilibrium (after a 4 hours contact). The final concentrations of ammonium and neodymium in solution were respectively 0.231 and 0.181 mol/L and the resin was converted up to 91.4%. The separation factor was expressed as follow:

$$\alpha_B^A = \frac{C_{res,NH_4} \times C_{sol,Nd}}{C_{res,Nd} \times C_{sol,NH_4}} = \frac{8.6}{91.4} \times \frac{3 \times 0.181}{0.231} = 0.221 \tag{40}$$

Mean values are used for interdiffusion coefficient either in the resin or in solution:

$$D = D_A D_B (z_A + z_B)/(z_A D_A + z_B D_B)$$

which gives for the resin : $D_{res} = 2.5\ 10^{-8} cm^2 s^{-1}$ and for solution $D_{sol} = 1.3\ 10^{-5} cm^2 s^{-1}$. The concentration of fixed ionic groups C_{res} was measured to be 5.8 meq/cm^3. The film thickness is considered to be close to 10^{-3} cm which is characteristics of a well-stirred solution. According to (Eq. (39)), the criterion becomes:

$$ratio = \frac{5.8 \times 2.5\ 10^{-8} \times 10^{-3}}{3 \times 0.1 \times 1.3\ 10^{-5} \times 0.035} \times (5 + 2 \times 0.221) \simeq 6\ 10^{-3}.$$

This value is greatly inferior to 1 which confirms that the rate is effectively controlled by particle diffusion in this particular case. The concentration range which corresponds to the particle diffusion control can also be roughly determined: the critical concentration is 1.7 10^{-3} eq/L which corresponds to 6 10^{-4} mol/L for neodynium. Below this concentration, the exchange may shift to film transfer.

6.2 Description of concentration profiles

The calculated concentration profiles in the resin and their evolution with time are plotted in Figure 6 for the proton/ammonium exchange and in Figure 7 for the ammonium/neodymium exchange. As remarked by Helfferich[15], the shape of the profile depends on the ratio of the diffusion coefficients between the ion rejected by the resin and the ion adsorbed. In both cases the faster ion is initially found in the resin but the ratio of diffusion coefficients are different. In the first case, the ratio $D_{H^+}/D_{NH_4^+}$ is close to 1.6 while the ratio $D_{NH_4^+}/D_{Nd^{3+}}$ is close to 13 in the second case. The concentration of the faster ion will stay large in the resin and become smaller near the surface. The interdiffusion then decreases towards the center. The more important is the ratio between the diffusion coefficients, the quicker the outer shells is depleted compared to the rest of the resin. In the second case a sharper boundary is then formed.

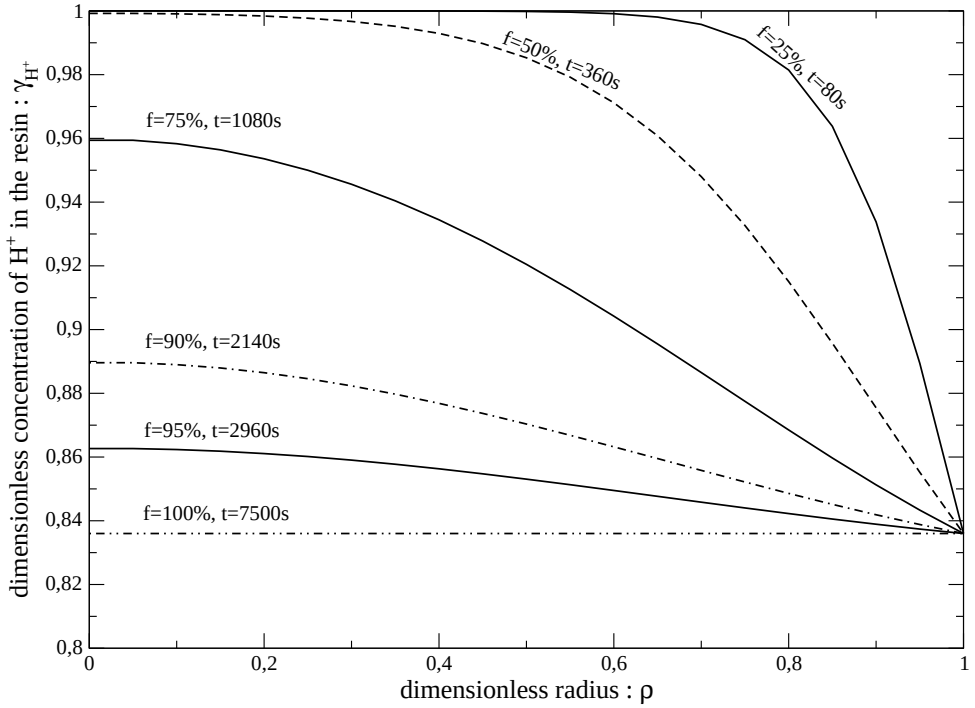

(a) H^+ concentration profile

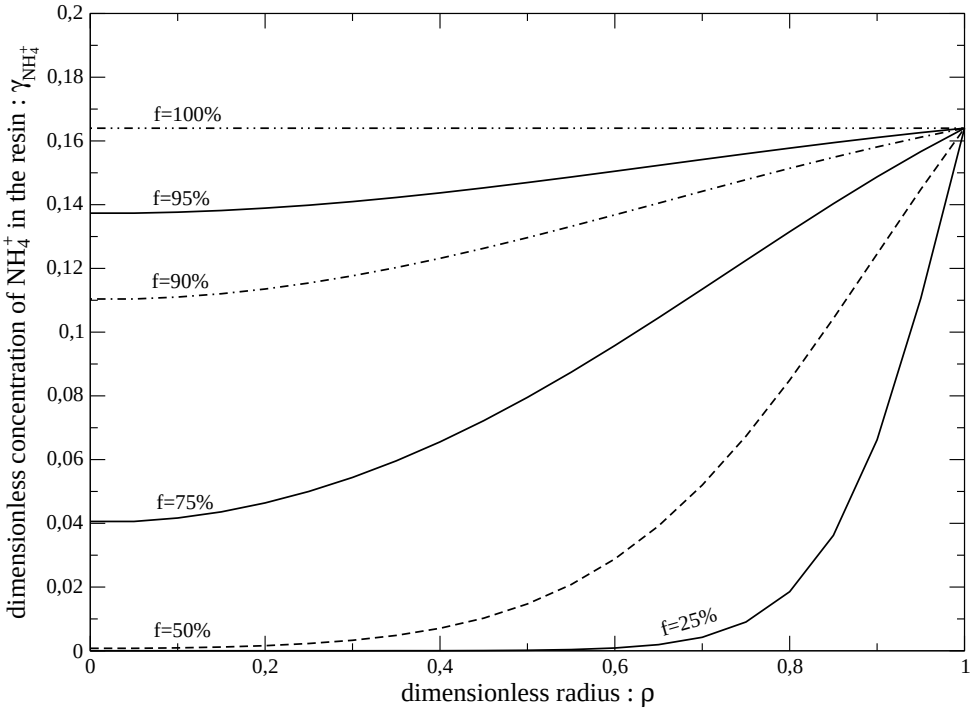

(b) NH_4^+ concentration profile

Figure 6: Concentration profiles in the resin for the proton/ammonium exchange.

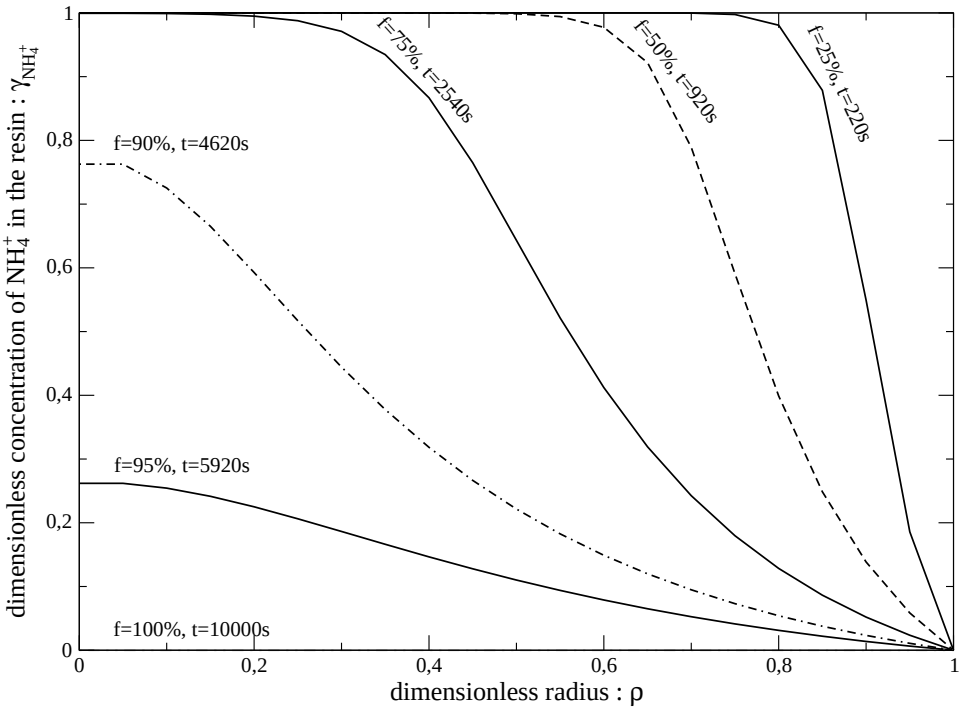

(a) NH_4^+ concentration profile

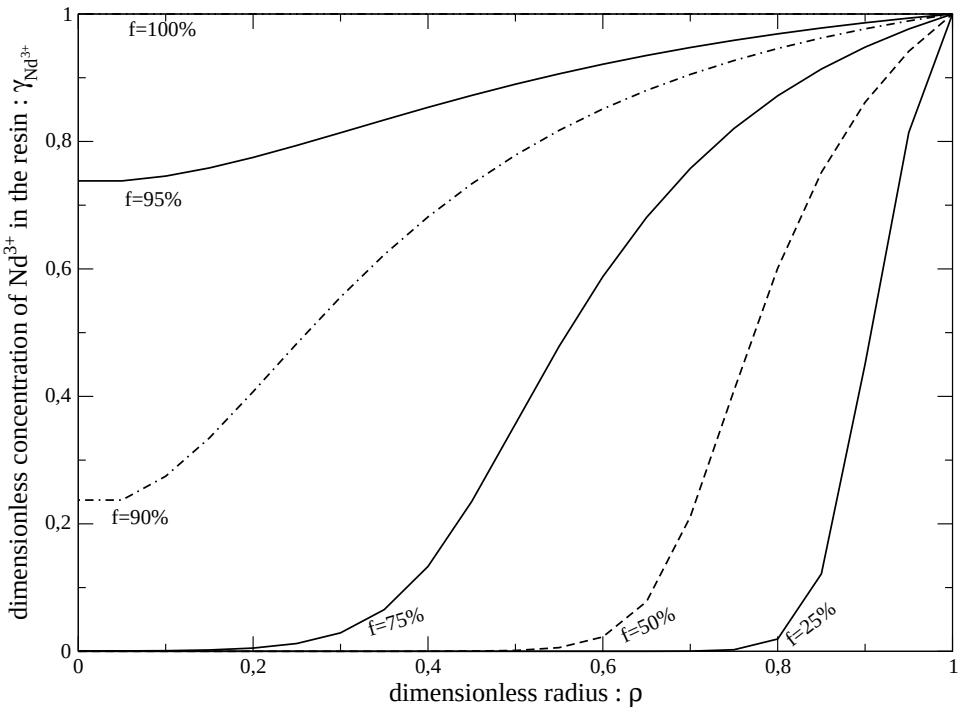

(b) Nd^{3+} concentration profile

Figure 7: Concentration profiles in the resin for the ammonium/neodymium exchange.

We introduce the notion of inhomogeneity factor defined by

$$\frac{|\gamma_A(0,\tau) - \gamma_A^\infty|}{|\gamma_A^0 - \gamma_A^\infty|} \tag{41}$$

This inhomogeneity factor will evolve differently according to the ratio of mobilities of the exchanging cations, see Figure 8.

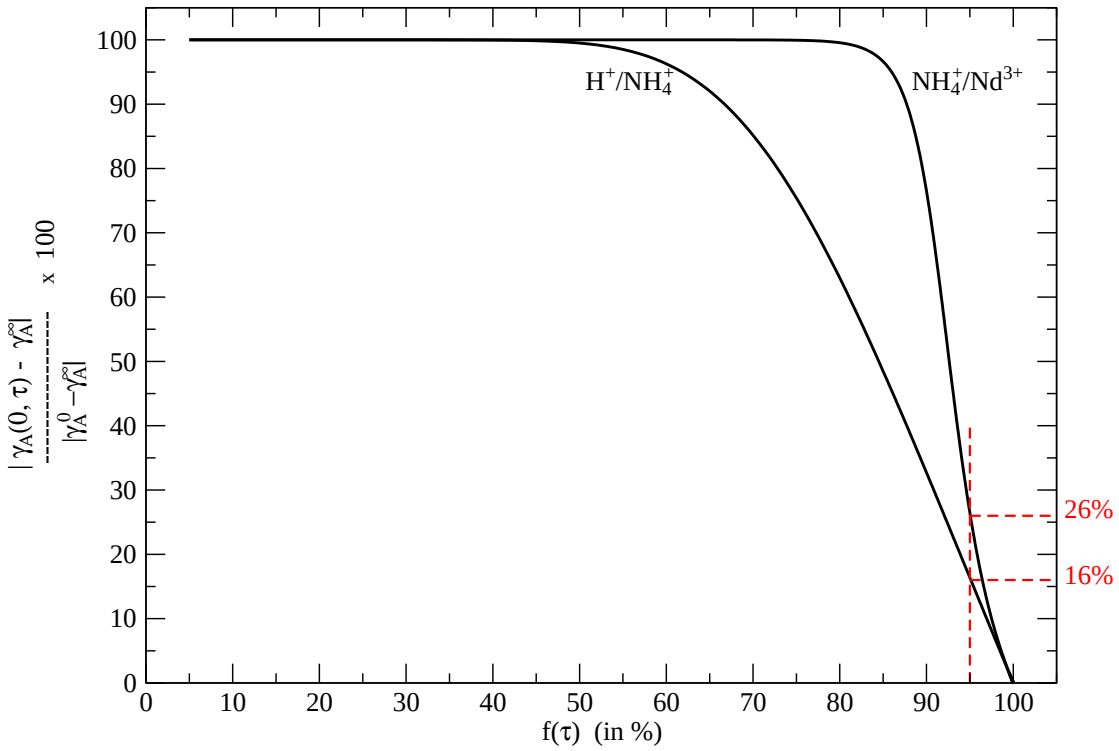

Figure 8: Representation of the homogeneity factor versus the fractional attainment of equilibrium for the two exchanges studied in a carboxylic resin.

For example, for a fractional attainment of equilibrium of 95%, an inhomogeneity factor of 16% is found for the first exchange while 26% is obtained for the second exchange. The more important is the ratio of diffusion coefficients between the ion rejected by the resin and the ion adsorbed, the more important is the inhomogeneity factor for a same fractional attainment of equilibrium.

However, in order to reach a full homogeneity in the resin (less than 5% inhomogeneity factor), a 100% achievement is necessary: the time required will depend on the mobilities of both cations and on the direction of the exchange (forward or backward).

Conclusion and perspectives

This preliminary work shows that it is possible to extract self diffusion coefficients of two counter ions in an ionic exchange resin by fitting the exchange kinetics through a semi-implicit numerical resolution of the Nersnt-Planck equation and an optimization procedure. This modelling was applied to monovalent-monovalent cations exchange but also to monovalent-trivalent cations exchange and allowed to determine the self diffusion coefficients of H^+, NH_4^+ and Nd^{3+} in a carboxylic resin. Those parameters are fundamental for modelling and describing the evolution of the fractional attainment of equilibrium with time for an exchange implying trivalent lanthanide with microspheres of carboxylic resin. Above all, it allows to determine the concentration profile in the resin and to check the full achievement of the reaction and the homogeneity of a lanthanide distribution inside the kernel for a given time of contact.

In further works, more experimental data has to be measured. Hence classical efficient optimization methods could be used, which would even more decreases the calculation time required for the optimization. Moreover, the rate of convergence and the results reliability of the optimization process could be improved by giving weight factors for each experimental data. These weight factors should be linked to the measurement uncertainties and would be taken into account through the error calculation. Eventually, this approach could be applied to the treatment of ionic exchange with resin in finite solution volume conditions which can be encountered in batch experiments. In this case, the time variation of concentrations in solution has to be taken into account. The distribution ratio will play an important role in the determination of self diffusion coefficients.

Acknowledgement

The authors thank C. Faivre-Pierret and A. Meunier for participating to the experimental acquisitions. D. Lacoume and E. Debier from Rohm & Haas Company are also acknowledged for supplying samples of resin and for fruitful discussions. The authors want also to thank the referees for their relevant comments.

List of symbols

Real	Dimensionless	Signification
r_0		radius of the resin,
r	ρ	radial coordinate,
t	τ	time,
RH		resin in its proton form,
n		number of equivalent,
Q	q	amount of specie,
Q_{max}		full exchange capacity,
F	f	fractional attainment of equilibrium,
C	γ	concentration,
C_{max}		total equivalent concentration,
D		individual diffusion coefficient,
z		electrochemical valence,
	λ	distribution ratio.

The subscripts A and B refer to the counter ion species. The superscript 0 (resp. ∞) corresponds to an evaluation of the variable at initial time (resp. equilibrium time).

References

(1) Xiong, C.; Yao, C.; Wang, L.; Ke, J. *Hydrometallurgy* **2009**, *98*, 318–324.

(2) Coca, M.; Mato, S.; González-Benito, G.; Ángel Urueña, M.; García-Cubero, M. *Journal of Food Engineering* **2010**, *97*, 569–573.

(3) de Dardel, F.; Arden, T. V. *Ion Echangers*; Ullmann's Encyclopedia of Industrial Chemistry; Wiley, 2001.

(4) Riveros, P. A. *Hydrometallurgy* **2004**, *72*, 279–290.

(5) Pesavento, M.; Biesuz, R. *Analytical and Bioanalytical Chemistry* **2003**, *376*, 1023–1029.

(6) Harbour, R. M.; Hale, W. H. *Radiochem. Radioanal. Letters* **1972**, *10*, 339–344.

(7) Chattin, F. R.; Benker, D. E.; Lloyd, M. H.; Orr, P. B.; Ross, R. G.; Wiggins, J. T. *Transplutonium Elements - Production and Recovery*; ACS Symposium Series, 1981; Vol. 161, pp 173–185.

(8) Weber, G. W.; Beatty, R. L.; Tennery, V. J. *Nuclear Technology* **1977**, *35*, 217–226.

(9) Notz, K. J.; Haas, P. A.; Shaffer, J. H. *Radiochimica Acta* **1978**, *25*, 153–160.

(10) Hunt, R. D.; Lindemer, T. B.; Hu, M. Z.; DelCul, G. D.; Collins, J. L. *Radiochimica Acta* **2007**, *95*, 225–232.

(11) Fernandez, A.; McGinley, J.; Somers, J.; Walter, M. *Journal of Nuclear Materials* **2009**, *392*, 133–138.

(12) Mokhtari, H. Ph.D. thesis, Université Paris XI Orsay, 2008.

(13) Rengaraj, S.; Moon, S.-H. *Water Research* **2002**, *36*, 1783–1793.

(14) Boyd, G. E.; Adamson, A. W.; L. S. Myers, J. *J. Am. Chem. Soc.* **1947**, *69*, 2836–2848.

(15) Helfferich, F.; Plesset, M. *The journal of chemical physics* **1958**, *28*, 418–424.

(16) Dickinson, E. J. F.; Freitag, L.; Compton, R. G. *J. Phys. Chem. B* **2010**, *114*, 187–197.

(17) Marhol, M. *Ion Echangers in Analytical Chemistry. Their Properties and Use in Inorganic Chemistry*; Elsevier, 1982; Vol. XIV.

(18) der Lee, J. V. *Thermodynamic and mathematical concepts of CHESS*; Technical Report, 1998.

(19) Helfferich, F. *J. Phys. Chem* **1962**, *66*, 39–44.

(20) Helfferich, F. *Ion Exchange*; Mc Graw Hill, 1962.

(21) Nernst, W. *Z. Physik Chem. (Leipzig)* **1889**, *4*, 129–181.

(22) Planck, M. *Ann. Physik* **1890**, *39*, 161–186.

(23) Plesset, M.; Helfferich, F.; Francklin, J. *The journal of chemical physics* **1958**, *29*, 1064–1069.

(24) Courant, R.; Friedrichs, K.; Lewy, H. *IBM Journal* **1967**, 215–234, *English translation of the 1928 German original, Math. Ann 100(32)*.

(25) Ciarlet, P. *Basic error estimates for elliptic problems*, North-Holland, Amsterdam ed.; Handbook of Numerical Analysis (P.G. CIARLET & J.-L. LIONS, Editors), 1991; Vol. II : Finite Element Methods (Part I), pp 17–351.

(26) Hackbusch, W. *Series in computer mathematics, Springer-Verlag* **1985**.

(27) Van Der Vost, V. *SIAM J. Sci. Stat. Comput.* **1992**, *13*, 631–644.

(28) Boyd, G. E.; Soldano, B. *J. Am. Chem. Soc.* **1954**, *75*, 6091–6099.

(29) Vanysek, P. *Handbook of Chemistry and Physics*; D. R. Lide, CRC Press, 1992.

(30) Soldano, B. *Annals New York Academy of Sciences* **1953**, *57*, 116–124.

Graphical TOC Entry

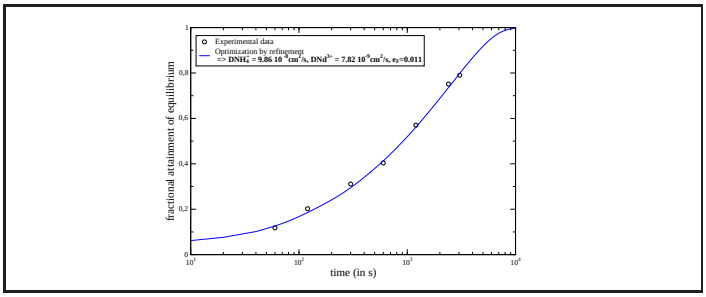

Experimental and modelized fractional attainment of equilibrium in a carboxylic resin during an ammonium/neodymium exchange.